J Mater Sci (2007) 42:6325–6330
DOI 10.1007/s10853-006-1253-7

Spatially resolved luminescence properties of ZnO tetrapods

Cordt Zollfrank · Carlos R. Rambo · Miroslaw Batentschuk · Peter Greil

Received: 11 October 2006 / Accepted: 10 November 2006 / Published online: 24 April 2007

Abstract ZnO tetrapods were prepared by Zn-vapour deposition at 740 °C in Argon and subsequent oxidation in air for 1–30 min. The photoluminescence (PL) and cathodoluminescence (CL) spectra were measured from ZnO particles collected at various distances from the Zn source representing decreasing dimensions. The ZnO tetrapods showed a green emission centred at 516 nm (2.40 eV) band and the exciton emission at 387 nm (3.20 eV). The measured data suggested that the green emission is strongly increased for particle sizes below 500 nm, whereas the exciton emission is dominant for particle size larger than 500 nm. Spatially resolved CL-measurement on individual tetrapod legs showed, that the green emission increases with decreasing ZnO leg diameter. To our knowledge, the local CL spectroscopic measurements were correlated with the dimensions of the individual ZnO tetrapods for the first time.

C. Zollfrank (✉) · P. Greil
Department of Materials Science and Engineering, Glass and Ceramics, University of Erlangen-Nuremberg, Martensstrasse 5, Erlangen 91058, Germany
e-mail: cordt.zollfrank@ww.uni-erlangen.de

C. R. Rambo
Graduate Program on Materials Science and Engineering – PGMAT, Department of Chemical Engineering – EQA, Federal University of Santa Catarina, P.O. Box 476, Florianopolis, SC 88040-900, Brazil

M. Batentschuk
Department of Materials Science and Engineering, Electrical Engineering Materials, University of Erlangen-Nuremberg, Martensstrasse 7, Erlangen 91058, Germany

Introduction

Zinc oxide (ZnO) is a well known semiconductor with a wide-band gap (3.37 eV) and a large exciton binding energy of 60 meV [1]. ZnO exhibits an efficient blue-green emission at room temperature and can be used for a large variety of applications in optical, electronic short wavelength devices and lasers [2, 3]. Current investigations concerning the synthesis of ZnO have been focused mainly on the production of nanostructured ZnO [4] such as nanowires, nanotubes, nanobelts or nano-tetrapods and whiskers [5–9]. Different methods to produce nano-structured ZnO from various substrates were reported, including mixtures of ZnO and carbon [10], thermal evaporation of metallic Zn and subsequent oxidation [11–13], chemical vapour deposition [6] and thermal decomplexation of aqueous Zn-salt solutions [14, 15]. Patterned arrays can be manufactured using vapour-phase transport process to grow ZnO nanowires [1]. Zn-vapour deposition with subsequent oxidation was shown to be the simplest method for the synthesis of ZnO nanoparticles as well for the synthesis of micro-sized ZnO [16]. For 1D or 3D ZnO particles such as whiskers or tetrapods (T-ZnO) a vapour–solid growth mechanism was proposed [17]. The T-ZnO morphology strongly depends on the partial pressures of Zn and O_2, as well as on the distance of the substrate from the Zn evaporation source [10]. Recent reports on the optical properties of nano-scaled ZnO particles with different morphologies, such as microcages [18], nanobelts [6], whiskers [19] and tetrapods [20, 21] indicated their potential use as light-emitting devices in nanoscale opto-electronic applications.

The photo-excited green emission of a nanostructured ZnO particle depends on the morphology and the size [1, 19, 22, 23]. Decreasing the ZnO nanorod diameter from

120 nm to 30 nm results in a drastically increase of the green photoluminescence (PL) intensity [1]. However, the lateral resolution of the exciting laser beam is usually limited to 1 μm due to optical limitations. Even established scanner systems for the digital radiography allow the acquisition of the local luminescence intensity of the area of 20 μm under optimised conditions [24]. Cathodoluminescence (CL) microscopy is a very efficient non-destructive technique which provides a detailed analysis and spatial resolution of luminescent properties of micron-sized particles [25]. CL measurements also allows the evaluation the near-band edge luminescence and luminescent properties related to surface defects of semiconductor materials [26]. In particular, CL spectroscopy on ZnO nanostructures in the scanning electron microscope (SEM) allows a topographic image of the emission region of a particle [27]. Furthermore, CL microscopy is an excellent tool for luminescence mapping and for selective area studies on emitting nanostructures with a high lateral and depth resolution. First low temperature CL investigations on individual ZnO nanowires grown by vapour–liquid–solid (VSL) method allowed a detailed view on the peak structure [28]. CL studies on elongated ZnO micro- and nanostructures prepared by sintering of ZnO powders exhibited a strong enhancement of the green luminescence compared to bulk ZnO, where the green emission was negligible [29]. Until now, the relationship between structural dimensions of the T-ZnO and their PL and CL properties is currently unclear. We report on the optical properties of ZnO tetrapods (T-ZnO) synthesised by Zn-vapour release up to 700–800 °C in argon atmosphere and subsequent oxidation in air to form the T-ZnO. The measured PL and CL intensities were correlated to the dimensions of the T-ZnO microstructure.

Experimental part

The ZnO tetrapods (T-ZnO) were obtained by Zn-vapour release in argon atmosphere and subsequent oxidation in air. Zn powder (0.3–1.5 mm, 99.9%, Merck, Germany) was placed in an Al_2O_3 crucible. A polycrystalline alumina (α-Al_2O_3) substrate was then fixed above the Zn bed where the growth of ZnO occurred. The system was inserted in an electrically heated tube furnace and heated up to 700–800 °C in flowing argon atmosphere. After a dwell time of 1–30 min the gas-inlet was opened for air flow into the tube to form ZnO. The samples were collected as a white solid at different distance from the Zn source. The microstructure of the ZnO was characterised by scanning electron microscopy (SEM Phillips XL 30, The Netherlands) equipped with an energy dispersive X-ray analysis (EDX, INCA x-sight, Oxford Analytical Instruments Ltd., UK). The phase composition, the crystalline structure, as well as the crystallite size of the specimens were determined by X-ray diffractometry (XRD) using CuK_α radiation at a scan rate of $0.75°min^{-1}$ over a 2θ range of 20–80° (D 500, Siemens, Germany).

The photoluminescence (PL) spectra were recorded at room temperature with a fluorescence spectrometer (J&M, Germany) equipped with fibre optics for excitation and detection of the emission. The ZnO samples were placed on a flat substrate and illuminated at an angle of 45° and a distance of approximately 5 mm from the powder surface. Excitation wavelengths of 320 and 350 nm with an integration time of about 500 ms were applied. The emission was detected (J&M, TIDAS MMS/16, Germany) at an angle of 45° relative to the substrate surface between 320 and 750 nm. The data were evaluated with the Fluoroscan software FL 3095 (J&M, Germany) and corrected for the intensity of the Si detecting array using correction files provided by the software. The areas of the peaks were calculated fitting a Gauss curve to the measured data using the PeakFit v4 software (SPSS Inc., USA). The ZnO powders were placed on double-side adhesive carbon films on aluminium sample holders and analysed in a SEM (Jeol JSM-6400, Japan). The cathodoluminescence (CL) spectra were recorded with a front illuminated UV CCD chamber Jobin Yvon, type MTECCD-1024x128-6 mounted at the monochromator (Jobin Yvon, model Triax 320, France) outside the operating vacuum chamber. A photomultiplier (R1463 13 mm, Hamamatsu, Japan) with a detection range of 300–600 nm and a maximum sensitivity at 420 nm was used for the CL-images. The SEM was operated at 20 kV with a current of 0.1–1 nA. Spikes in the spectra as a result of pixel faults in the detector were not removed. The areas of the peaks were calculated fitting a Gauss curve to the raw data using the PeakFit v4 software (SPSS Inc., USA).

Results and discussion

Figure 1 shows SEM-micrographs of the microstructure of the ZnO formed after 10 min oxidation at 750 °C at different sampling distances from the Zn source. The surface of the Zn-melt was set as reference distance ($d = 0$). The ZnO crystals found close to the Zn evaporation source (Zn-melt, d~0) exhibited a broad variety of morphologies, varying from platelets to rods and irregular shapes with varying sizes from 1 μm to several tenths of micrometers (Fig. 1a). However, some nano-size ZnO filament and T-ZnO like structures were also found. The formation of micron-sized T-ZnO was observed beginning at a distance of approximately 10 cm from the Zn-melt surface (Fig. 1b). Needle-like ZnO crystals in addition to hexagonal rods with diameters of approximately 1 μm are also

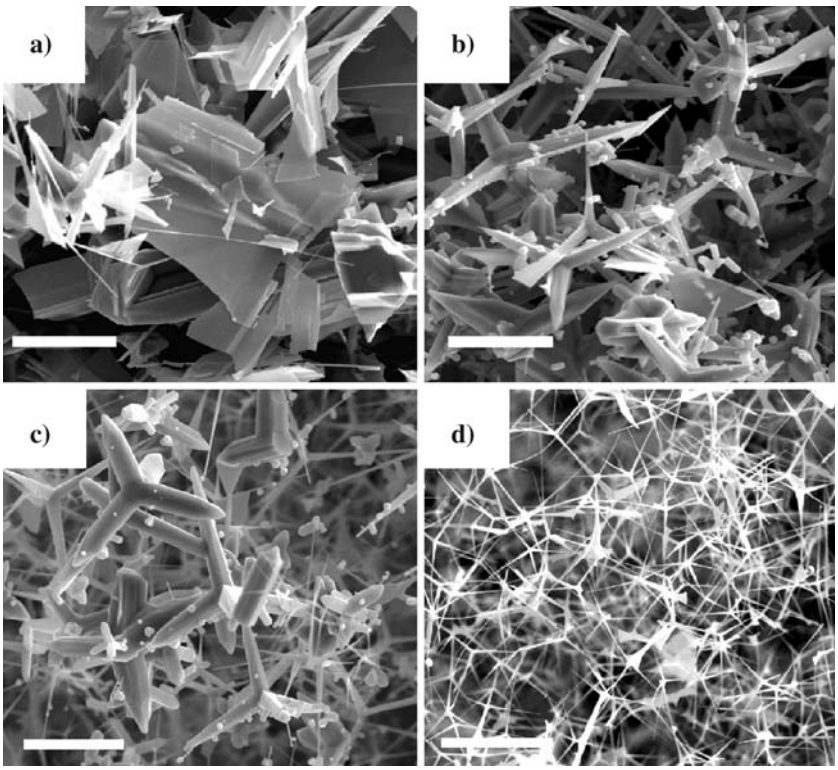

Fig. 1 SEM-micrographs of the ZnO structures formed by oxidation of Zn collected at various distances d from the Zn source: (**a**) $d = 0$, (**b**) $d = 10$, (**c**) $d = 13$, and (**d**) $d > 15$ cm; the scale bar represents 10 μm

present. At a distance of approximately 13 cm most of the ZnO particles exhibited tetrapod-like shapes (Fig. 1c). ZnO rods and T-ZnO with leg diameters of around 200 nm and lengths of up to several tenths of micrometers were also observed. The fraction of T-ZnO increased at a formation distance exceeding 15 cm, where almost exclusively a tetrapod morphology was found. The legs of the tetrapods exhibited diameters ranging from 100 nm to 600 nm with overall lengths of several tenths of micrometres (Fig. 1d). It can be deduced from this observation that the average structural dimensions decrease with increasing sampling distance from the Zn source.

X-ray diffraction patterns of ZnO powders were measured to examine the crystal structure of the obtained micro and nanoparticles. All samples produced gave similar XRD patterns indicating the high crystallinity of the ZnO particles. The polycrystalline ZnO formed on the surface of the substrates had a typical hexagonal structure, characterised by a strong (101) diffraction peak. Lattice parameters $a = 0.3243$ nm and $c = 0.5216$ nm of the hexagonal lattice were calculated from the XRD data, which corresponds well with the data published in the literature [1, 20, 21]. Additional element characterisation by EDX confirmed the sole presence of Zn and O in the samples.

Figure 2 shows the results of the PL and CL measurements obtained from the powders sampled at the various distances from the Zn source. A strong UV-peak centred at 387.2 nm (3.20 eV) assigned to the near-band gap exciton emission was observed in all PL-spectra obtained from the ZnO powder regardless of the distance from the Zn source (Fig. 2a). The green emission usually found between 470 nm and 570 nm was not detected for the specimens sampled up to a distance of 10 cm from the Zn source. This distance is related to structural dimensions of the ZnO particles ranging from one up to several micrometers. As the fraction of sub-micron sized ZnO increases and T-ZnO structures emerge with the increasing distance from the Zn source, Fig. 1c, d, a green emission centred at 516 nm (2.40 eV) appeared in the PL-spectra. The relative intensity of the green emission compared to the exciton related UV-emission is stronger than the UV-emission for samples collected at 15 cm, which were mainly composed of T-ZnO with leg diameters below 1 μm. An occasionally observed blue band centred at 480 nm due to the existence of oxygen-depletion interface traps in ZnO films and nanostructures [20, 30] was not found for the obtained T-ZnO. A similar behaviour described for the PL was observed in the CL-spectra measured from the same samples (Fig. 2b). The UV-peak was located at 387 nm (3.20 eV). The green emission centred at 525 nm (2.36 eV) was only detected for the ZnO sampled at distances larger than 10 cm from the Zn source. The observed intensity of the green peak was lower than the UV emission in all CL-spectra. Additionally, a small blue emission at 480 nm (2.58 eV) accompanied the green peak. However, the blue peak was also absent in micron-sized ZnO particles sampled below 10 cm.

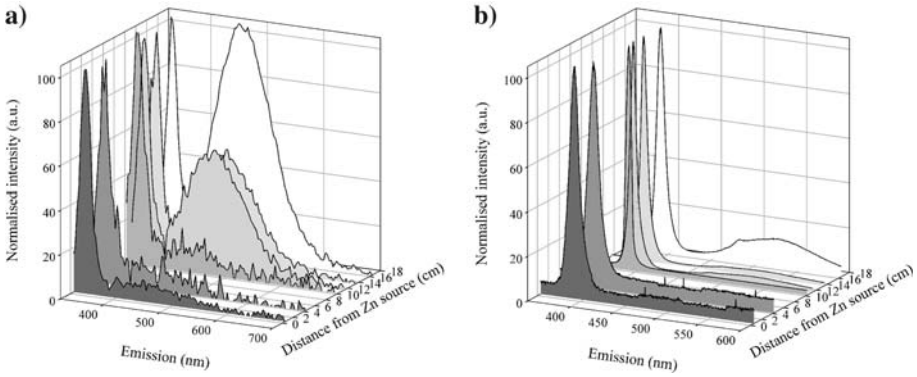

Fig. 2 Optical properties of the reaction formed ZnO as a function of the sampling distance d from the Zn source: (**a**) PL-emission spectra recorded at an excitation wavelength of 320 nm, (**b**) CL spectra measured at an acceleration voltage of 20 kV; the peaks were normalised to the exciton emission

Our results confirmed that the green emission should vary with the position along the tetrapod leg as a function of the leg diameter [1, 19, 22, 28, 29]. Since the diameter of the leg is larger at the origin compared to its end, the relative intensity of the green emission is expected to be lower at the origin increasing towards the end of the leg. This issue was evidenced by spatially resolved CL-measurements on a typical tetrapod leg of 13 μm in length shown in Fig. 3. The leg diameter was 1.25 μm at the origin decreasing to 0.64 μm at the end. CL-spectra were obtained along the tetrapod leg on the areas highlighted by circles in Fig. 3a. The intensities of the measured spectroscopic data were normalised to the intensity of the UV-emission (Fig. 3b). The strong exciton emission centred at 380 nm (3.20 eV) was observed in all CL-spectra along the tetrapod leg. However, the CL-intensity of the green peak increased when the leg diameters were smaller than 1 μm. The maximum intensity of the green emission was measured in the spectrum recorded at the end of tetrapod where the leg diameter was 0.64 μm. Grym et al. showed, that the ratio of maxima of the UV- to the green intensities approximately corresponds to the ratio of intensities of these bands on the outer area of ZnO tubes with nearly the same dimensions [29]. The bang gap emission observed at 377.5 nm (3.29 eV) for ZnO nanorods with a diameter of 35 nm shifted to 372.1 nm (3.32 eV) as the nanorods decreased to 8 nm. In our CL-data, the exciton peak shifted from 389.9 nm (3.18 eV) at a leg diameter of 1240 nm to 386.9 nm (3.20 eV) for a diameter of 640 nm (Fig. 3c).

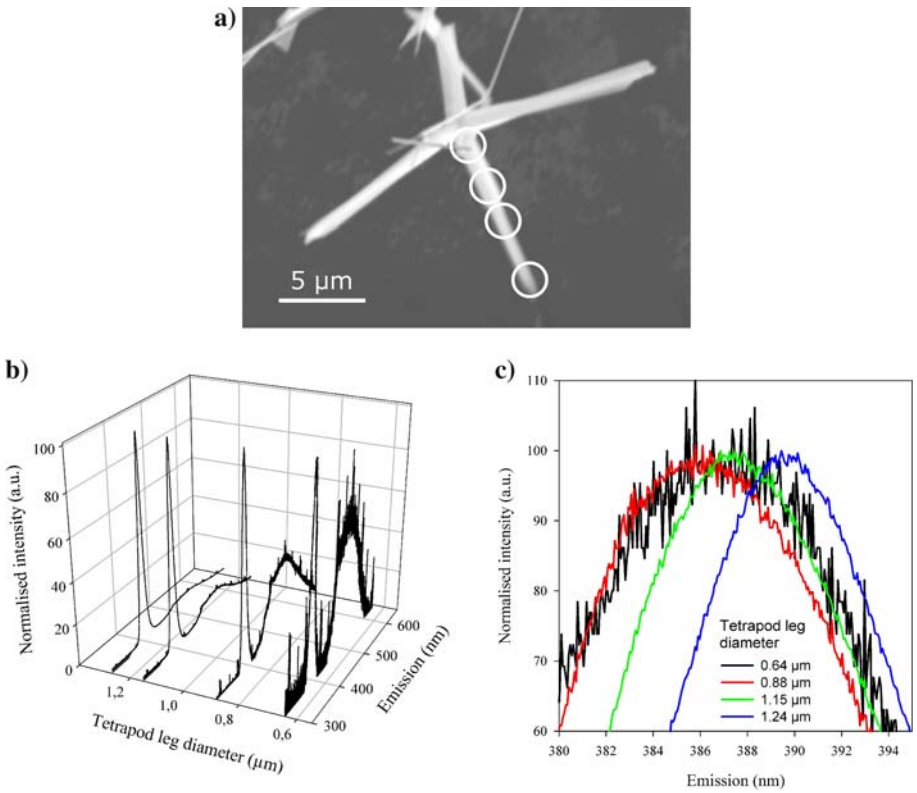

Fig. 3 Cathodoluminescence analysis from the leg of a ZnO tetrapod: (**a**) SEM image of the ZnO tetrapod, the circles indicate the regions where the CL-spectra were recorded, (**b**) CL-spectra along the ZnO tetrapod leg as function of leg diameter; the peaks were normalised to the exciton emission, (**c**) magnification of the exciton emission highlighting the blue shift along the tetrapod leg

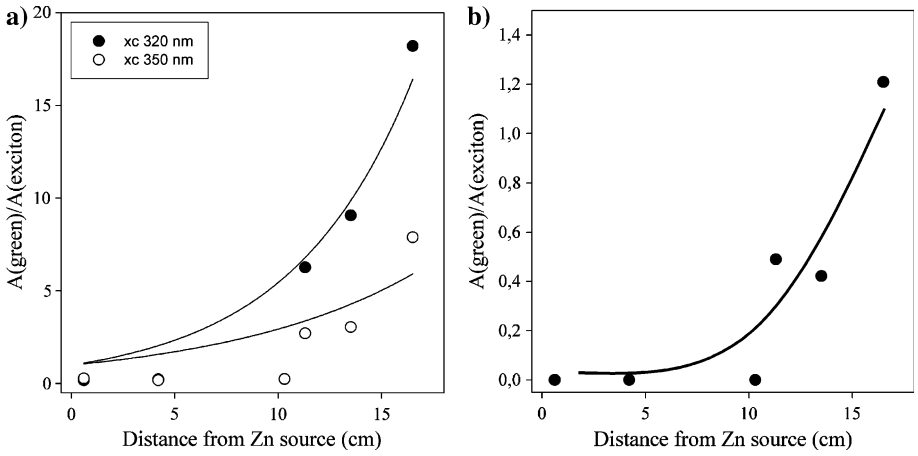

Fig. 4 Ratios of the peak areas *A*(green)/*A*(exciton) plotted as a function of the sampling distance *d* from the Zn source for (**a**) emission spectra recorded at excitation wavelengths of 320 nm and 350 nm and (**b**) cathodoluminescence measurements; the lines are drawn as a guide for the eye

The PL and the CL-intensity of the green emission is dependent on the morphology and size of a single ZnO particle. In Fig. 4a, the ratio of the green and UV luminescence intensities is shown as a function of the sampling distance from Zn source. The phenomenon of the dependence of the green emission on the size was already described in the literature [1, 19, 22]. It was observed that the decrease of the diameter of a ZnO nanorod yields a strong increase of the green PL-intensity. The difference in the green emission intensity was attributed to the different surface to volume ratio, which is larger in the nanowires suggesting a higher concentration of oxygen vacancies on the particle surface [1]. However, most of the recent studies used wavelengths of photons with energies higher than the energy of the band gap, e.g. 281 nm [22], 325 nm (He–Cd laser [1, 28]) or Xe-lamps [21] for excitation of the PL-emission. Here, two different excitation wavelengths are used, 320 nm and 350 nm. The ratio of the peak areas of the green and the UV-emission *A*(green)/*A*(exciton) obtained from Gauss fitting imply that the UV-emission is strong for small values, whereas the green emission dominates at higher values. The results were plotted as a function of the distance from the Zn source for both wavelengths (Fig. 4a). The green emission strongly emerges after 11 cm distance from the Zn source with *A*(green)/*A*(exciton) larger than 2:1. It is an interesting fact, that this ratio is apparently larger for an excitation wavelength of 320 nm compared to the excitation at 350 nm in all cases. The ratio for the T-ZnO structures found at 15 cm was 8:1 for 350 nm excitation and 18:1 for 320 nm excitation. Thus, the green emission is significantly enhanced with decreasing excitation wavelengths [1, 21, 22]. The electron transition from the valence band (VB) to the conduction band (CB) at excitation energies larger then the band gap is the origin of all emissions [31]. Our experimental data suggest that excitation of electrons into the lower exciton energy levels is preferred at 350 nm, yielding a decreased intensity of the green PL and the UV-emission is preferred. At 320 nm excitation, the separation of charge carriers is facilitated, because the electron is more likely to be excited from the VB to higher energy level of the CB border. The probability of locating electrons and holes for radiative recombination increases, favouring the green emission over the near-band gap emission.

The same procedure for calculating the *A*(green)/*A*(exciton) ratio was applied for the CL-spectra (Fig. 4b). The shape of the curve was similar to the one described above for the PL emission. Starting from sampling distance of 10 cm, the green emission emerged and the ratio *A*(green)/*A*(exciton) rapidly increased. However, the calculated values of the ratio *A*(green)/*A*(exciton) were considerable lower compared to the values found in the PL measurements. The maximum ratio was 1.2:1 for sampling distances exceeding 15 cm, where the particles primarily consisted of T-ZnO. This could already be expected from the CL-spectra, where the UV emission was extremely large in all observed spectra compared to the green emission. A possible explanation might be the large energy density of the incident electron beam (20 kV). The number of exciton levels is virtually not limited and most of the acquired energy will be dissipated through the near-band gap emission. However, the maximum of the CL-intensity is restricted because the number of the available defects is finite.

Figure 5 shows the results of the CL measurements as a function of the tetrapod leg diameter. The diagram suggests that the exciton emission is dominant for leg diameters larger than 500 nm, characterised by small *A*(green)/*A*(exciton) ratios. If the leg diameter drops below 500 nm, the green emission becomes stronger. At leg diameters below 400 nm, the green emission is dominant in the CL leading to large values of *A*(green)/*A*(exciton) ratio. It was reported that the green light emission intensity increases relative to the UV emission as the ZnO rod diameter decreases from 100 nm to 50 nm, which was attributed to the occurrence of a significant high fraction of oxygen

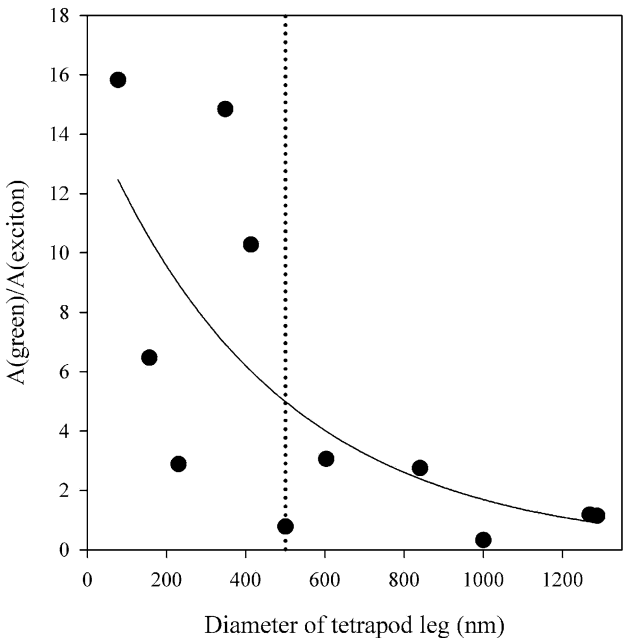

Fig. 5 (**a**) Ratios of the CL-peak areas *A*(green)/*A*(exciton) plotted as function of the T-ZnO leg diameter; the line is drawn as a guide for the eye

vacancies in the thinner nanowires [1]. As both emission processes are likely to compete with each other, it is assumed that the visible emission should involve a step in which the photo-generated hole is trapped efficiently somewhere in the particle. The rate of this hole trapping must be much faster than the radiative recombination rate of the exciton emission [22]. Trapping of a generated hole at the surface is therefore consistent with the observed size-dependence on the emission intensities. The rate of a surface trapping process decreases as the particle size increases, since the surface to bulk ratio decreases.

Conclusions

The PL and CL characteristics of ZnO microstructures and ZnO tetrapods were evaluated as a function of particle dimensions. Spatially resolved CL measurements showed that the green emission strongly increases when the size of the ZnO particles decreases below 500 nm. The ratio *A*(green)/*A*(exciton) was significantly increased with decreasing tetrapod leg diameter. Simultaneously, the exciton emission exhibited a blue-shift. The luminescence properties of ZnO nanostructures can be tuned by controlling the size of ZnO microstructures.

Acknowledgements The authors are grateful to E. Völkl for the technical assistance on the CL-measurements. Financial support of the German Science Foundation (DFG) and the University of Erlangen-Nuremberg is gratefully acknowledged. C.R. Rambo thanks CNPq-Brazil for the financial support.

References

1. Huang MH, Wu Y, Feick H, Tran N, Weber E, Yang P (2001) Adv Mater 13:113
2. Huang MH, Mao S, Feick H, Yan H, Wu Y, Kind H, Weber E, Russo R, Yang P (2001) Science 292:1897
3. Reynolds DC, Look DC, Jogai B (1996) Solid State Comm 99:873
4. Xu C, Kim M, Chun J, Kim DE (2005) Nanotechnology 16:104
5. Lyu SC, Zhang Y, Ruh H, Lee HJ, Shim HW, Suh EK, Lee CJ (2002) Chem Phys Lett 363:134
6. Zhang J, Yu W, Zhang L (2002) Phys Lett A 299:276
7. Chen Z, Shan Z, Cao MS, Lu L, Mao SX (2004) Nanotechnology 15:365
8. Tseng YK, Huang CJ, Cheng HM, Lin IN, Liu KS, Chen IC (2003) Adv Funct Mater 13:811
9. Kong XY, Ding Y, Yang R, Wang ZL (2004) Science 27:1348
10. Leung YH, Djurisic AB, Gao J, Xie MH, Chan WK (2004) Chem Phys Lett 385:155
11. Wan Q, Song ZT, Liu WL, Lin CL, Wang TH (2004) Nanotechnology 15:559
12. Dai Y, Zhang Y, Bai YQ, Wang ZL (2003) Chem Phys Lett 375:96
13. Park J, Choi HH, Siebein K, Singh RK (2003) J Cryst Growth 258:342
14. Vayssieres L (2003) Adv Mater 15:464
15. Govender K, Boyle D, Kenway PB, O'Brien P (2004) J Mater Chem 16:2575
16. Yan H, He R, Pham J, Yang P (2003) Adv Mater 15:402
17. Dai Y, Zhang Y, Li QK, Nan CW (2002) Chem Phys Lett 358:83
18. Fan HJ, Scholz R, Kolb FM, Zacharias M, Gösele U (2004) Solid State Comm 130:517
19. Gao T, Huang Y, Wang T (2004) J Phys Cond Mater 16:115
20. Yu WD, Li XM, Gao XD (2004) Chem Phys Lett 390:296
21. Dai Y, Zhang Y, Li QK, Nan CW (2002) Chem Phys Lett 375:83
22. Van Dijken A, Meulenkamp EA, Vanmaekelbergh D, Meijerink A (2000) J Lum 87–89:454
23. Zhong H, Wang J, Pan M, Wang S, Li Z, Xu W, Chen X, Lu W (2006) Mat Chem Phys 97:390
24. Li H, Hackenschmied P, Epelbaum B, Batentschuk M (2002) Mat Sci Eng B Solids B94:32
25. Urbieta A, Fernández P, Piqueras J, Hardalov C, Sekiguchi T (2001) J Phys D Appl Phys 34:2945
26. Fernández P, García JA, Remón A, Piqueras J, Muñoz V, Triboulet R (1998) Semicond Sci Tech 13:410
27. Saito N, Haneda H, Koumoto K (2004) Microelectr J 35:349
28. Lorenz M, Lenzer J, Kaidshev EM, Hochmuth H, Grundmann M (2004) Ann Phys (Leipzig) 1–2:39
29. Grym J, Fernández P, Piqueras J (2005) Nanotechnology 16:931
30. Wu JJ, Liu SC (2002) Adv Mater 14:215
31. Lima SAM, Sigoli FA, Jafelicci M Jr, Davolos MR (2001) Int J Inorg Mat 3:749